Evaluating Sulfur-Tolerance of Metal/$Ce_{0.80}Gd_{0.20}O_{1.90}$ Co-Impregnated $La_{0.20}Sr_{0.25}Ca_{0.45}TiO_3$ Anodes for Solid Oxide Fuel Cells

Robert Price [a*], Jan G. Grolig [b], Andreas Mai [b] and John T. S. Irvine [a]

[a] School of Chemistry, University of St Andrews, St Andrews, Fife, KY16 9ST, UK
[b] HEXIS AG, Zum Park 5, CH-8404 Winterthur, Switzerland

Abstract

The Ni-based cermet Solid Oxide Fuel Cell (SOFC) anode is prone to poisoning by sulfur-based odourising agents, and naturally occurring sulfur species, present in unprocessed natural gas feeds. Next generation SOFC anodes should be able to withstand exposure to these poisons in the event of a malfunction or breakdown of desulfurisation units. Here, we present results pertaining to the sulfur-tolerance of Ni/$Ce_{0.80}Gd_{0.20}O_{1.90}$ (CGO), Pt/CGO and Rh/CGO co-impregnated $La_{0.20}Sr_{0.25}Ca_{0.45}TiO_3$ anode 'backbone' microstructures and their ability to recover performance after being exposed to H_2S. The Ni/CGO co-impregnated system exhibited severe poisoning by H_2S, however, the Rh/CGO system displayed good stability in Area Specific Resistance (ASR) upon introduction of 1-2 ppm of H_2S and the Pt/CGO system showed minimal increases in ASR with the addition of 1-8 ppm H_2S. Recovery measurements performed in non-humidified H_2 at 300 mA cm^{-2}, after exposure to 8 ppm H_2S, indicated that the Pt/CGO and Rh/CGO systems could recover within 10 minutes, whilst 60 minutes were required to achieve almost a full recovery of performance for the Ni/CGO system. Additionally, all three impregnate systems showed good stability in operating voltage, after an initial drop, in a fuel gas containing simulated syngas (2:1 H_2:CO) with 8 ppm H_2S.

Keywords

Solid Oxide Fuel Cell; Anode; Lanthanum Strontium Calcium Titanate; Impregnation; Sulfur-Tolerance

1. Introduction

Solid Oxide Fuel Cells (SOFC) are energy conversion devices which allow useful electrical currents to be produced as a result of electrochemical oxidation of a fuel gas, e.g. H_2 or CH_4. Currently, the state-of-the-art SOFC anode material is the Ni-based ceramic-metal composite or cermet. Despite its widespread use in the SOFC industry, redox instability, issues with Ni agglomeration and its propensity to coke and/or poison, in unprocessed natural gas feeds, are key areas for improvement in 'next-generation' anodes.

In our previous work, SOFC containing single-phase $La_{0.20}Sr_{0.25}Ca_{0.45}TiO_3$ ($LSCT_{A-}$) anode 'backbone' microstructures, co-impregnated with a variety of transitional/platinum group metals and $Ce_{0.80}Gd_{0.20}O_{1.90}$ (CGO), have shown very promising performances during short-term electrochemical testing in 97 % H_2/3 % H_2O [1]. For example, a SOFC containing a

Rh/CGO co-impregnated $LSCT_{A-}$ anode gave an Area Specific Resistance (ASR) of 0.62 Ω cm^2 at 850 °C.

In addition to assessing the performance of the aforementioned SOFC anodes in 'clean' and commonly used fuel streams, it is desirable to characterise them in non-ideal fuel gases to determine their stability towards effects such as sulfur poisoning and their ability to oxidise typical reformate gases such as syngas (a 2:1 ratio of H_2:CO). These test conditions are especially important in the event of desulfurisation unit malfunction or expiry, within SOFC-based systems, when sulfur-containing species may reach the anode for short periods of time. Specifically, it is important to test SOFC using representative concentrations of sulfur-based odourising agents that can be found in Western European natural gas grids (between 1.4 and 14 ppm [2]). This is the region in which HEXIS' micro-combined heat and power (μ-CHP) units currently operate.

Therefore, here we present results relating to the short-term testing of SOFC containing: Ni/CGO, Pt/CGO and Rh/CGO co-impregnated $LSCT_{A-}$ anodes in fuel streams of non-humidified H_2 (99 % H_2:1 % H_2O) and simulated syngas (2:1 H_2:CO), containing between 1 ppm and 8 ppm H_2S.

2. Experimental

2.1 SOFC Fabrication

Electrolyte-supported SOFC were produced using thick-film ceramic processing techniques, as previously reported [1,3,4], though the procedure is briefly outlined here. A $La_{0.20}Sr_{0.25}Ca_{0.45}TiO_3$ ($LSCT_{A-}$, Treibacher Industrie AG) ink was deposited onto one side of the pre-sintered 6 molar (mol.) % scandia-stabilised-zirconia (6ScSZ, HEXIS) electrolyte, using screen printing. The anode was dried at 80 °C, before being sintered at 1350 °C for 2 hours in air. A state-of-the-art LSM-YSZ cathode was screen printed onto the opposite side of the electrolyte using a single layer of composite ink (50:50 wt. % $(La_{0.80}Sr_{0.20})_{0.95}MnO_3$ (LSM, Praxair Specialty Ceramics):8 mol. % yttria-stabilised-zirconia (8YSZ, Daiichi Kigenso Kagaku Kogyo Co. Ltd)) to form an electrochemically active functional layer, followed by a double layer of pure LSM ink for current collection. Cathodes were sintered at 1100 °C for 2 hours in air. Both electrodes had an active area of 1 cm^2 after sintering.

2.2. Anode Catalyst Co-Impregnation

$LSCT_{A-}$ anode microstructures were decorated with electrocatalytically active coatings of $Ce_{0.80}Gd_{0.20}O_{1.90}$ (CGO) and nanoparticles of Ni, Pt or Rh. This was achieved using the process of catalyst co-impregnation. Initially, a nitrate precursor solution of CGO was prepared by dissolving the required molar ratios of $Ce(NO_3)_3.6H_2O$ and $Gd(NO_3)_3.6H_2O$ (99 %, Sigma-Aldrich) in ethanol. A drop of the solution was added to the surface of the $LSCT_{A-}$ anode and was allowed to diffuse into the microstructure, before the solvent was evaporated at 80 °C and the nitrate precursors were decomposed, to form the metal oxide, at 500 °C for 30

minutes in air. This process was repeated until the desired weight percentage of CGO (with respect to the $LSCT_{A-}$ anode 'backbone' mass) had been obtained. The same process was then used to add the transition/platinum group metal (PGM) oxide catalyst phase to the anode microstructure. Here, the $Ni(NO_3)_3.6H_2O$ precursor (99 %, Acros Organics) was dissolved in ethanol, whilst nitric acid-based solutions of $H_2[Pt(NO_3)_6]$ and $Rh(NO_3)_3$ (Johnson Matthey) were diluted with ethanol to improve the wetting of the solutions on the $LSCT_{A-}$ anode microstructure.

2.3. SOFC Testing Procedure

Au meshes, spot welded to Au wires, were used as current collectors for both fuel and air electrodes. The meshes were attached to the surface of the electrodes using small spots of Au paste (M-9875, Metalor Technologies (UK) Ltd.) and good adhesion was achieved after firing at 750 °C for 30 minutes in air. SOFC were installed vertically into a 'sealless' setup with alumina felt gas diffusion gaskets, allowing the creation of a post-cell combustion zone; an analogous environment to that experienced by HEXIS SOFC. SOFC were tested at 850 °C with a total fuel flow rate of 250 mL min^{-1} and a compressed air flow rate of 250 mL min^{-1}. After initial characterisation was carried out in non-humidified H_2, H_2S was introduced to the fuel stream, as a poisoning agent, at concentrations of 1 ppm, 2 ppm, 4 ppm, 6 ppm and 8 ppm; a particularly relevant protocol as the concentration of sulfur-based odourising agents reaching the SOFC stack is expected to slowly increase as monolayer adsorption of the balance of plant (BoP) components within the system is achieved. A recovery measurement was performed in non-humidified H_2 (after poisoning with H_2S) by operating the SOFC galvanostatically for between 10 and 60 minutes. Finally, the fuel gas composition was changed to simulated syngas, with a 2:1 ratio of H_2:CO, containing 8 ppm of H_2S. AC impedance spectra were collected at 0.7 V bias, with a 50 mV excitation amplitude, and galvanostatic measurements were performed at 300 mA cm^{-2}, using a Solartron SI 1280B Electrochemical Measurement Unit.

2.4. Post-Mortem Scanning Electron Microscopy

Tested SOFC were broken to reveal a full cross section for Scanning Electron Microscopic (SEM) analysis. The broken samples were mounted vertically on an Al sample stub, using Ag paint (Agar Scientific, G3691) to provide a rigid bond to the holder and also to reduce charging of the samples. Subsequently, the samples were sputtered with a conductive carbon coating to further prevent charging, using a Quorum Q150R ES Rotary Pumped Coater. The thickness of the carbon coating was approximately 300 Å thickness (blue in colour), according to Kerrick *et al* [5]. Secondary and backscattered electron micrographs of the overall anode microstructure and magnified regions of the nanostructure were captured using a FEI Scios Dualbeam Focus Ion Beam (FIB)-SEM.

3. Results

3.1 Catalyst Loadings

The weight loadings for the Ni/CGO, Rh/CGO and Pt/CGO anode catalyst systems are presented in table 1. All anodes contained 15 weight (wt.) % CGO, which provides electrocatalytic activity toward the oxidation of the fuel gas, mixed ionic and electronic conductivity and a stabilising layer onto which the metallic catalyst particles are able to anchor. The metallic catalyst phases (Ni, Pt and Rh) provide the majority of the electrocatalytic activity for fuel oxidation and so lower loadings, than the CGO component, are typically employed. However, as Ni is a relatively poor catalyst in comparison to the PGMs, a higher loading (5 wt. %) was required than for Pt and Rh (2 wt. %).

Table 1. Loadings of co-impregnated anode catalysts employed in SOFC testing.

Anode Catalyst System	CGO Loading/wt. %	Metal Loading/wt. %
Ni/CGO	15	5
Pt/CGO	15	2
Rh/CGO	15	2

3.2 Characterisation of Performance in H_2S-Containing Fuels

3.2.1 AC Impedance Spectroscopy

Figure 1 and figure 2 display the complex plane and Bode format AC impedance spectra, respectively, obtained for the SOFC containing the Ni/CGO co-impregnated $LSCT_{A-}$ anode. The initial spectrum, taken in non-humidified H_2, indicates that a higher than expected ohmic resistance (R_s) (0.33 Ω cm^2) was achieved, due to imperfect contacting of the electrodes and the resistive contribution from the $LSCT_{A-}$ anode 'backbone' [1], with an ASR of 0.74 Ω cm^2. Details of equivalent circuit fitting for analogous SOFC are reported elsewhere [1], however, a short description of the discernible processes is given here. Three processes can often be observed in the AC impedance spectra of these SOFC and the possible assignments are as follows (at 850 °C and 0.7 V, in non-humidified H_2): i) a high-frequency anode charge transfer process (R_{p1}, f_{max} = 1002-502 Hz), ii) a mid-frequency cathode related process (R_{p2}, f_{max} = 50 Hz) and iii) a low-frequency gas conversion process (R_{p3}, f_{max} = 2-4 Hz). It is important to note that if the R_{p1} process is particularly dominant for a given catalyst system, the R_{p2} process may not be visible in the AC impedance spectrum [1]. In this case, the Ni/CGO anode catalyst system exhibits all three processes, though the R_{p2} process is largely masked by the R_{p1} process, effectively producing an elongated arc (figure 1). The introduction of 1 ppm H_2S causes a 0.06 Ω cm^2 increase in ASR, solely due to the increase in the polarisation resistance of the anode charge transfer arc. R_{p1} increases as a function of increasing H_2S concentration and results in an ASR of 0.90 Ω cm^2, in the fuel stream containing 8 ppm H_2S. This indicates that the Ni/CGO catalyst system is not able to operate in any fuel stream containing ppm

levels of sulfur-containing species, without a substantial degradation in ASR and, therefore, performance. A recovery measurement was taken, after galvanostatic operation, in order to assess the ability of the catalyst to recover. Operation of the SOFC at 300 mA cm^{-2} for 60 minutes, was required to reduce the ASR to 0.78 Ω cm^2; 0.04 Ω cm^2 higher the than the ASR obtained from the initial measurement in non-humidified H_2. It is noted that due to the gradual reduction of the $LSCT_{A-}$ backbone (indicated by the decrease in R_s between the initial and recovery measurements), this ASR upon full recovery would be slightly smaller than for the initial measurement. Subsequently, switching to simulated syngas with 8 ppm H_2S caused a further increase in R_{p1}, giving an ASR of 1.00 Ω cm^2. A more detailed discussion of the performance of all three anode catalyst systems in simulated syngas and 8 ppm H_2S will be provided subsequently.

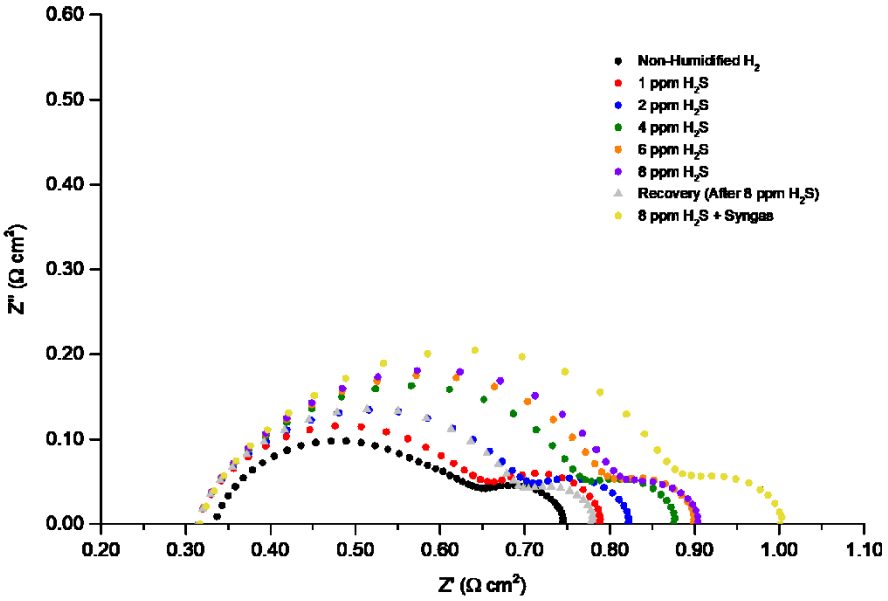

Figure 1. Complex plane AC impedance spectra collected for the SOFC containing a Ni/CGO co-impregnated $LSCT_{A-}$ anode in fuel gases containing H_2S.

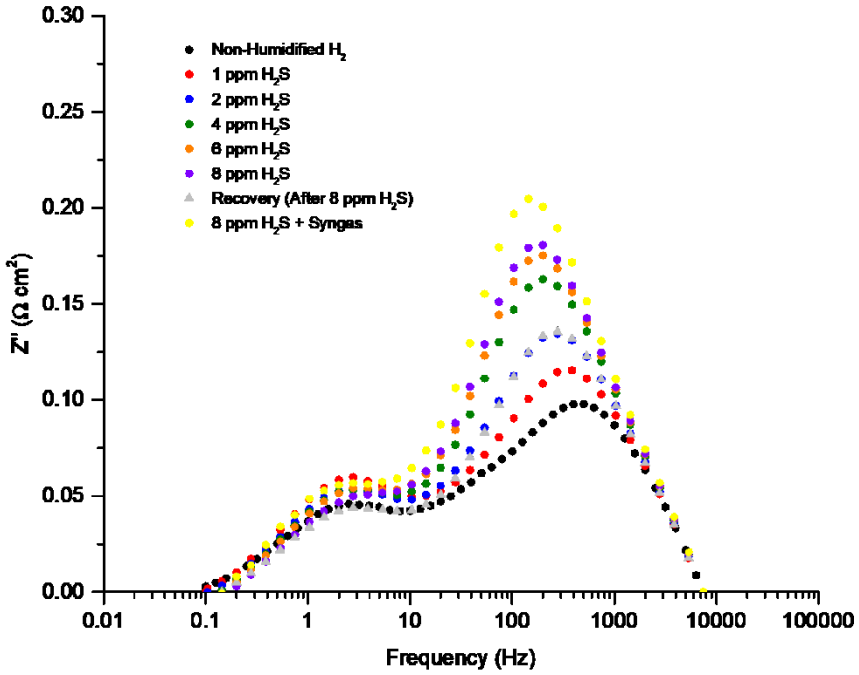

Figure 2. Bode format AC impedance spectra collected for the SOFC containing a Ni/CGO co-impregnated $LSCT_{A-}$ anode in fuel gases containing H_2S.

The complex plane and Bode format AC impedance spectra for the Pt/CGO catalyst system are shown in figures 3 and 4, whilst those pertaining to the Rh/CGO catalyst system are presented in figures 5 and 6, respectively. In similarity to the spectra collected for the Ni/CGO catalyst system, the R_{p1} and R_{p3} processes can be clearly identified for the PGM-containing catalyst systems. However, the Rh/CGO system more clearly shows the domain of the mid-frequency process, which has previously been attributed to a cathode contribution in these particular SOFC [1,6]. This process is discernible due to fact that the anode charge transfer process is much less resistive for the Rh/CGO co-impregnated $LSCT_{A-}$ anode and the frequency domains of the anode and cathode related processes no longer overlap. Despite both of these PGM-containing SOFC showing similar initial total polarisation resistances (~0.30 Ω cm^2), the Pt/CGO anode actually shows an improvement in performance upon introduction of 1-8 ppm of H_2S. In comparison, the Rh/CGO anode exhibits negligible increases in R_{p1} upon the introduction of 1-2 ppm H_2S, however, at concentrations between 4 and 8 ppm, larger increases in ASR are observed (e.g. a 0.06 Ω cm^2 increase with 8 ppm H_2S).

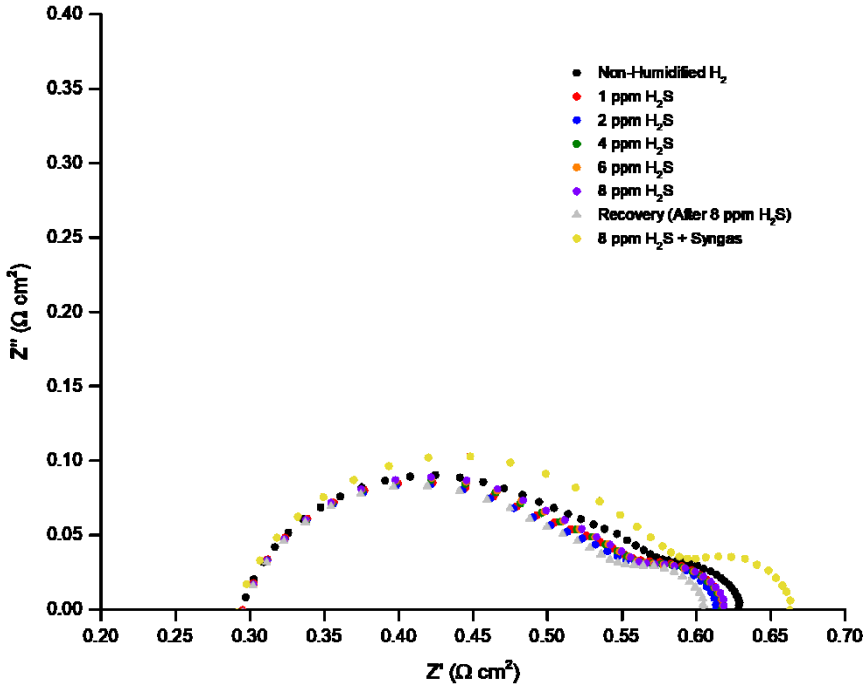

Figure 3. Complex plane AC impedance spectra collected for the SOFC containing a Pt/CGO co-impregnated $LSCT_{A-}$ anode in fuel gases containing H_2S.

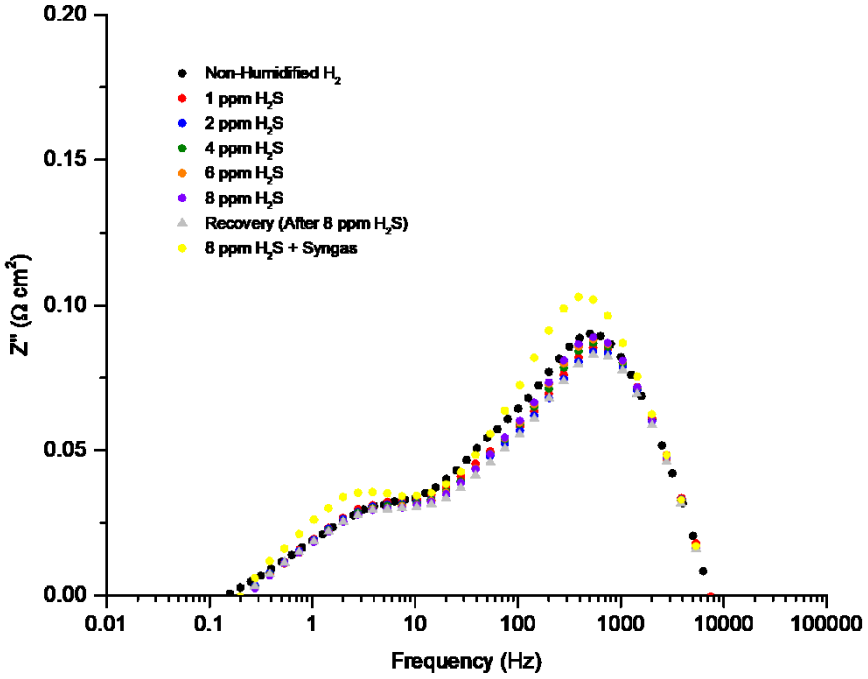

Figure 4. Bode format AC impedance spectra collected for the SOFC containing a Pt/CGO co-impregnated $LSCT_{A-}$ anode in fuel gases containing H_2S.

Crucially though, both of the PGM-containing anodes exhibit a full recovery and even an improvement in performance, in terms of ASR, after operation at 300 mA cm^{-2} for 10 minutes in non-humidified H_2. Therefore, these anodes would be able to withstand and recover quickly from exposure to sulfur-based odourising agents in fuel gas streams, in the event of a breakdown or malfunction of the desulfurisation units employed for fuel processing in SOFC-based systems. Switching from H_2 to simulated syngas (in the presence of 8 ppm H_2S) results

in a further increase of ASR for both SOFC, though the SOFC containing the Pt/CGO co-impregnated $LSCT_{A-}$ anode provides the lowest ASR under these conditions (0.66 Ω cm^2).

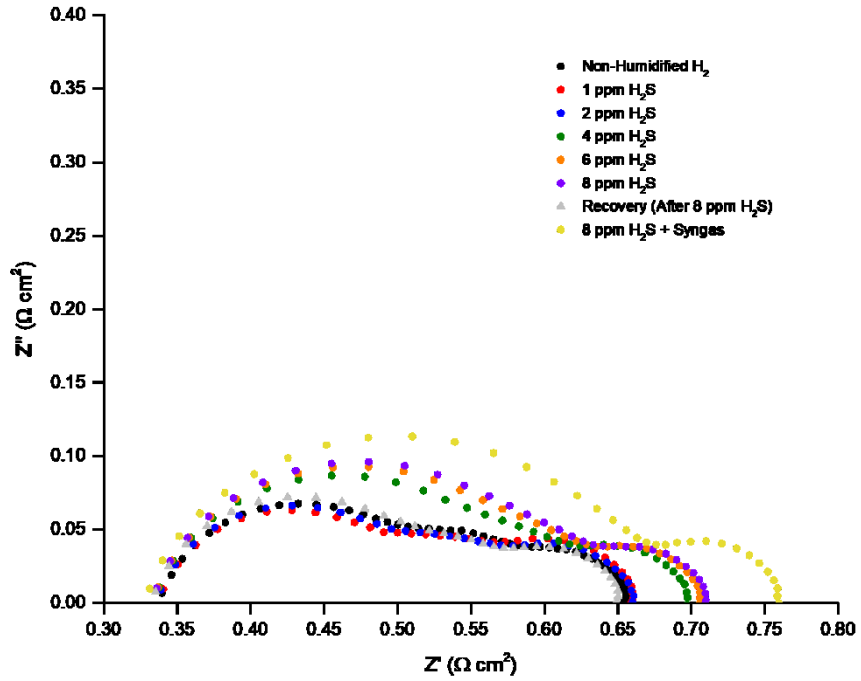

Figure 5. Complex plane AC impedance spectra collected for the SOFC containing a Rh/CGO co-impregnated $LSCT_{A-}$ anode in fuel gases containing H_2S.

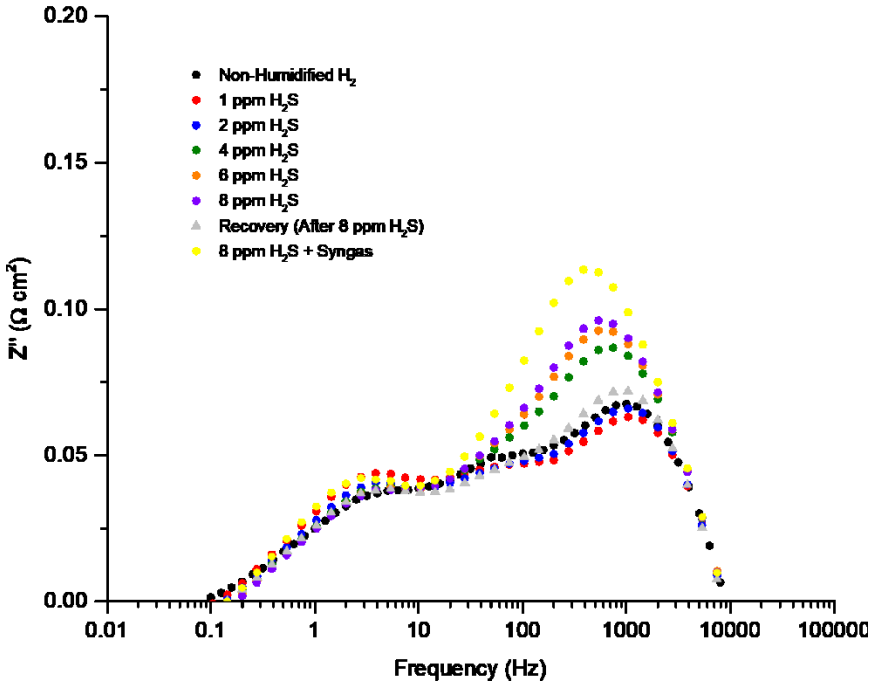

Figure 6. Bode format AC impedance spectra collected for the SOFC containing a Rh/CGO co-impregnated $LSCT_{A-}$ anode in fuel gases containing H_2S.

3.2.2 Short-Term Stability in Simulated Syngas with H_2S

In order to determine the stability of the Ni/CGO, Pt/CGO and Rh/CGO co-impregnated $LSCT_{A-}$ anodes in the event of the aforementioned fuel processing malfunctions, the SOFC were operated at 300 mA cm^{-2} for more than four hours in a fuel stream of simulated syngas with 8 ppm H_2S. Figure 7 shows the stability of the operating voltage as a function of operational time for all of the tested SOFC. The SOFC containing the Ni/CGO catalyst system showed the lowest operating voltage of the three cells, however, this voltage appeared to improve as a function of operational time. In contrast, both the Pt/CGO and Rh/CGO catalyst systems exhibited small initial reductions in operating voltage which subsequently stabilised during the test period. Ultimately, this shows that, irrespective of the 'baseline' performance in non-humidified H_2, all of the metal/metal oxide co-impregnated $LSCT_{A-}$ anodes presented in this research are capable of operating in Catalytic Partial Oxidation (CPOx) reformed natural gas containing typical levels of sulfur-based odourising agent used within Western European countries [2] for very short periods of time.

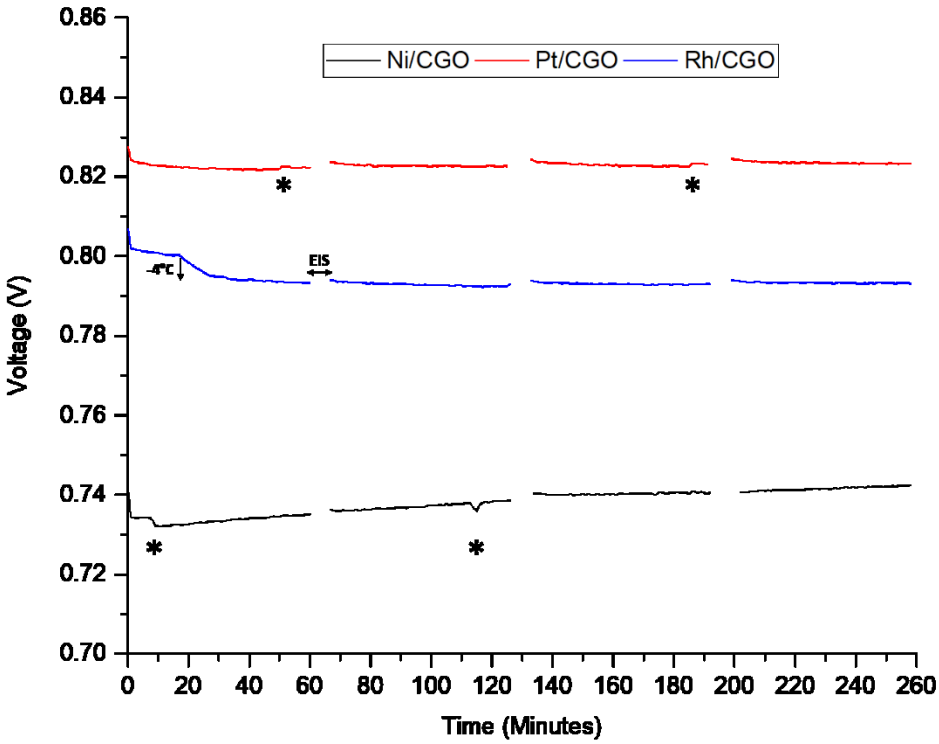

Figure 7. Plots of operating voltage versus time for SOFC containing: Ni/CGO, Pt/CGO and Rh/CGO co-impregnated $LSCT_{A-}$ anodes operating at 300 mA cm^{-2} in a fuel gas comprising a 2:1 ratio of H_2:CO with 8 ppm H_2S. Small variations in operating voltage, due to air compressor refills, are indicated by asterisks (*), whilst all other interruptions are due to the collection of electrochemical impedance spectra (EIS). The operating temperature of the SOFC containing the Rh/CGO catalyst system was corrected to 850 °C (by -4 °C) at the start of the operational period.

3.3 Post-Mortem Scanning Electron Microscopy

Figure 8 displays post-mortem scanning electron micrographs (SEM) of the broken cross-sections of all co-impregnated $LSCT_{A-}$ anodes, at low magnification. This overall aspect of the fuel electrodes highlights the similarity of the microstructure and impregnated nanostructure

within the Ni/CGO (figure 8a), Pt/CGO (figure 8b) and Rh/CGO-containing (figure 8c) anodes and indicates that the ceramic processing, in addition to the method of catalyst co-impregnation, is highly reproducible between samples. Furthermore, higher-magnification micrographs of regions of these anodes are provided in figure 9. Once again, common characteristics are identified between the Ni/CGO (figure 9 a), Pt/CGO (figure 9 b) and Rh/CGO (figure 9c) co-impregnated anodes, namely that the $LSCT_{A-}$ grains (dark grey) of the 'backbone' microstructure are coated with layers of impregnated CGO (brightly contrasting layers) which harbour fine nanoparticles of the metallic catalyst phase (brightly contrasting spots), which agrees well with previous research [1].

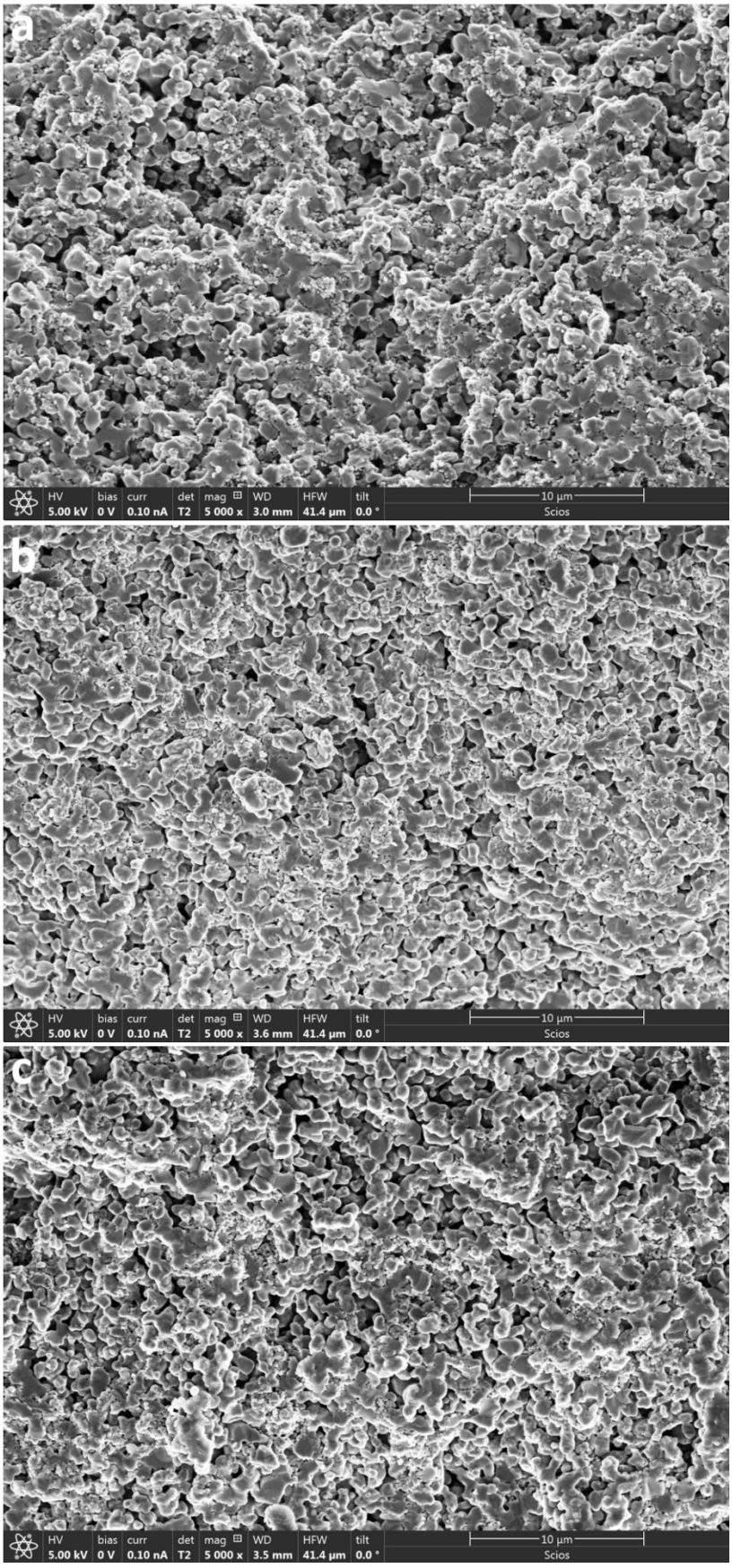

Figure 8. Secondary electron micrographs showing broken cross-sections of a) the Ni/CGO co-impregnated $LSCT_{A-}$ anode microstructure, b) the Pt/CGO co-impregnated $LSCT_{A-}$ anode microstructure and c) the Rh/CGO co-impregnated $LSCT_{A-}$ anode microstructure.

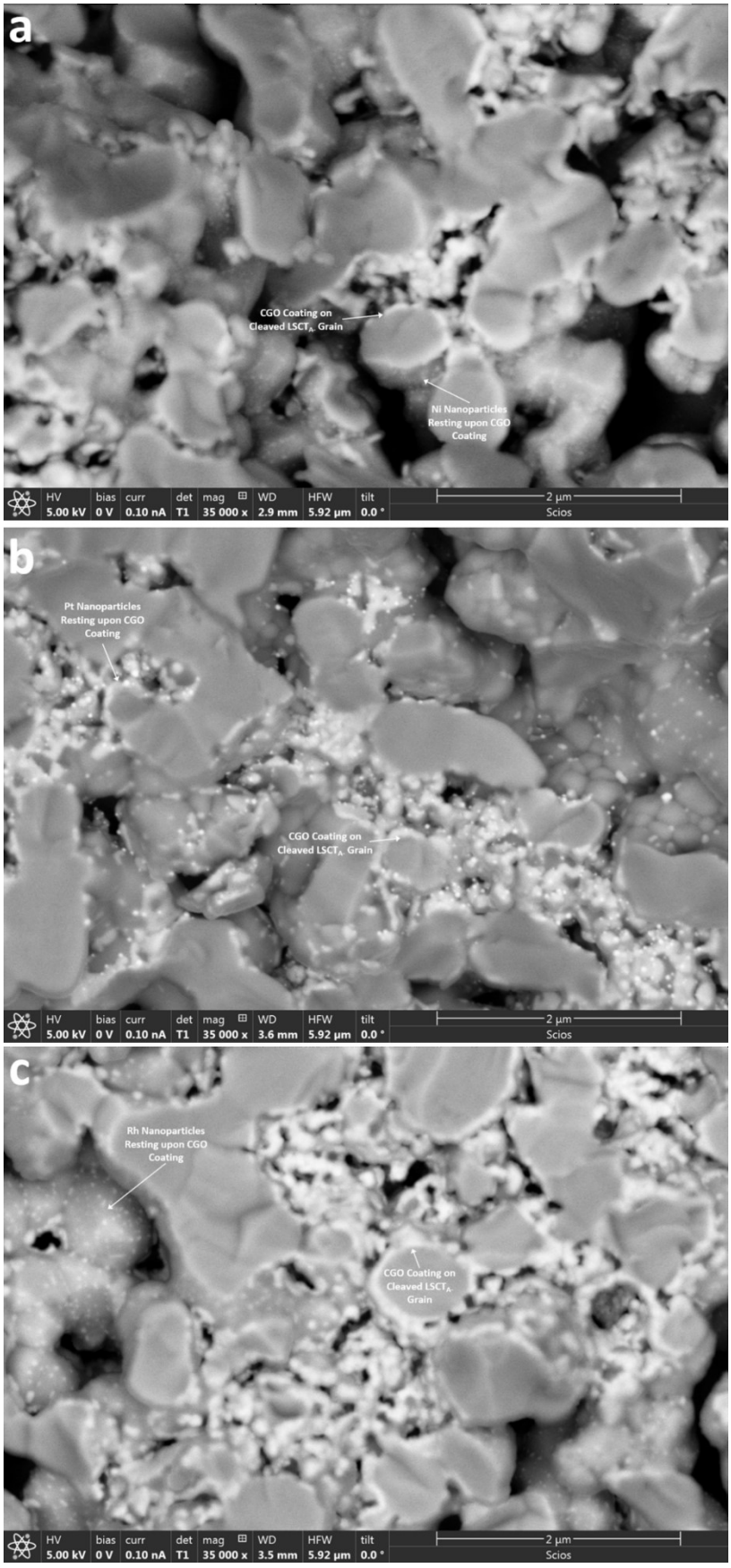

Figure 9. Backscattered electron micrographs of magnified regions of a) the Ni/CGO co-impregnated $LSCT_{A-}$ anode, b) the Pt/CGO co-impregnated $LSCT_{A-}$ anode and c) the Rh/CGO co-impregnated $LSCT_{A-}$ anode, showing metallic nanoparticles (brightly contrasting spots) resting upon layers of CGO which, in turn, coat grains of the $LSCT_{A-}$ 'backbone'.

4. Discussion

In non-humidified H_2, the main fuel oxidation process is believed to occur at the TPB between the impregnated metallic catalyst phase, the impregnated CGO coating (upon which they lie) and the fuel in the gas phase [1,7]. The SE micrographs presented in figure 9 confirm that a large proportion of the metallic catalyst nanoparticles rest upon the CGO component, which coats the grains of $LSCT_{A-}$ that form the conductive anode 'backbone'. Therefore, introduction of ppm concentrations of poisoning agents, *e.g.* H_2S, into the fuel stream may reduce the catalytic activity of the anode catalyst systems through adsorption on the active sites of the surface of the metallic component, the CGO component or both.

Firstly, considering the metallic catalyst phase, the Ni component is widely-reported to be readily poisoned by sulfur species [8–10], and can even form Ni_3S_2 intergrowths in the presence of high concentrations of H_2S [11]. Thus, it is unsurprising that the Ni/CGO catalyst system exhibited such severe poisoning in the presence of just 1 ppm H_2S, with further increases in anode charge transfer polarisation resistance being observed whilst increasing the H_2S concentration towards 8 ppm. In comparison, adsorbed sulfur species are also likely to inhibit the electrocatalytic activity of the Rh and Pt metallic catalyst phases; after all, the adsorption energies for H_2S and its constituents (e.g. atomic sulphur) are similar for Ni, Pt and Rh, as summarised by Cheng *et al*. [8].

However, the results presented here indicate that the Pt/CGO catalyst system remained almost unaffected by introduction of H_2S between 1 and 8 ppm, whilst the Rh/CGO catalyst was able to retain performance in 1 or 2 ppm H_2S, but in 4-8 ppm increases in anode charge transfer polarisation resistance were observed. Therefore, the differences in performance observed between the Ni/CGO, Pt/CGO and Rh/CGO anode catalyst system presented in this research must depend upon the mutualistic interaction between the metallic catalyst phase and the CGO component.

This mutualistic relationship was reported by Verbraeken *et al*. in a previous generation of research into these co-impregnated $LSCT_{A-}$ anodes [7], however, these relationships are also reported in the literature of fuel reforming catalysis for very similar catalyst systems. For example, Azad *et al*. reported that Rh catalysts supported on either CGO or CZO (cerium zirconium oxide) showed good stability and steam reforming activity towards toluene with 50 ppm H_2S (in comparison to catalyst systems containing alloyed Rh-Pd metallic nanoparticles) [12]. This stability was attributed to sulfidation of the ceria-based phase which may have acted as 'sacrificial' site for sulfur adsorption and reaction, allowing the Rh catalyst component to retain its catalytic activity [12]. Moreover, Lu *et al*. showed that a synergistic relationship exists between impregnated Pt nanoparticles and the $Ce_{0.80}Gd_{0.20}O_{1.90}$ support for the steam reformation of iso-octane containing 300 µg/g (300 ppm) of thiophene [13]. When changing the metallic catalyst phase for Ni, and also when replacing the CGO support for Al_2O_3, sulfur-tolerance was not observed, further confirming the existence of the synergistic relationship between the two components. The ability of CGO support to store

and release oxygen allowed the Pt catalyst to sequentially oxidise the thiophene and reduce water [13]. Specifically to SOFC, the CGO component present in Ni-CGO cermet anodes is known to form cerium oxysulfide species at the surface of the ceramic component, when exposed to sulfur-based poisoning agents, which have the ability to use O^{2-} anions to oxidise the sulfur species to SO_2 [14]. Zeng *et al*. showed that Ce_2O_2S could be reversibly formed from reduced CeO_2 (as an agent for desulfurising high-temperature gas) [15]; a phenomenon that may extend to CGO-containing cermet anodes. However, it should be noted that exposure to high concentrations of sulfur (e.g. >450 ppm) and formation of the Ce_2O_2S phase can result in anode degradation or deactivation, especially in co-impregnated SOFC anodes, as evidenced by the work of He *et al*. [16].

In contrast, the role of the $LSCT_{A-}$ anode 'backbone' in mitigating poisoning of the active electrocatalysts by sulfur species, is less well defined, especially in impregnated catalyst systems. Computational studies investigating the addition of basic oxides, such as CaO, BaO and SrO, to Ni-based SOFC anodes, suggest that the surface coverage of the Ni phase decreases as a result of the reduced sulfur chemical potential for bonding with such oxides [17]. Any Ca-O or Sr-O lattice terminations in the $LSCT_{A-}$ perovskite phase may, therefore, act as sites of preferential sulfur chemisorption, decreasing the surface coverage of sulfur on the active electrocatalyst phases [17]. Moreover, work by Marina *et al*. suggests that composite 'backbones' of lanthanum strontium titanate and cerium lanthanum oxide (LST-CLO), exposed to 75 ppm of H_2S, exhibited a low surface coverage (0.5) by chemisorbed sulfur, implying that, generally, these oxide-based anode materials adsorb H_2S less readily than typical Ni-YSZ anodes, for example [18].

Considering the AC impedance response of these metal/CGO co-impregnated $LSCT_{A-}$ anodes in simulated syngas with 8 ppm H_2S, further increases in the anode charge transfer process are observed when replacing the non-humidified H_2 fuel with a 2:1 mixture of H_2:CO. Performance of SOFC with commonly-employed Ni-based cermet anodes is reported to be similar regardless of whether the fuel gas used is H_2 or a CO/H_2 (reformed methane) mix, as shown by Weber *et al*. [19]. Therefore, similar responses are expected for the performance of the co-impregnated anodes presented here. The addition of H_2S to the simulated syngas mixtures, however, is also known to block the electrochemically active sites that facilitate H_2 oxidation and the water gas shift reaction (WGSR) [20], through which CO is oxidised, offering an explanation for the increased anode charge transfer resistance observed when switching from H_2 with 8 ppm H_2S to simulated syngas with 8 ppm H_2S. This is typically observed at high fuel utilisations [21] (employed to encourage the oxidation of H_2 and CO, rather than just the H_2 component), however it may be possible that this also occurs at the lower fuel utilisations employed here, to a lesser extent. Additionally, a small increase in the polarisation resistance of the gas conversion arc can be seen, most likely due to the difference in the gas composition under which this spectrum was collected.

Research performed by Bunluesin *et al*. into the effect of particle size, loading and platinum group metal type on the WGSR in metal/CeO_2 catalysts highlights several important factors which may also affect co-impregnated anodes containing similar metallic and ceria-based components. These reports suggest that different mechanisms of CO oxidation exist depending on the crystallite size of the ceria-based component. For example, the first mechanism (observed during reactions carried out at 240 °C – 300 °C) involves both the platinum group metallic phase as well as the supporting ceria component. Here, the metallic phase (Pt, Pd or Rh) is able to adsorb the CO, which is then oxidised by O^{2-} from the bulk of the ceria, in a bifunctional manner [22]. Subsequently, the ceria is reduced once again by any water present in the equilibrium gas mixture [22]. However, this pathway is only available if the crystallite size of the ceria is small, as larger crystals make reduction of the bulk ceria much more difficult. The kinetics of the WGSR for Pt, Pd or Rh supported on CeO_2 were found to be effectively identical, further implying that the mutualistic relationship between these two catalyst components and the interfacial active sites formed between them are crucial in determining the exact mechanism through which the WGSR proceeds. In the case that large crystals of CeO_2 are present, the second mechanism of CO oxidation, employing only the metallic catalyst phase, will ensue [22]. This is likely to be the predominant mechanism occurring in the co-impregnated $LSCT_{A-}$ anodes operating at high temperature (presented in this work). However, the aforementioned mutualistic relationship that arises at interfacial sites between the metallic catalyst phase and the CGO component may play an important role in the WGSR and, therefore, may well experience slightly different effects of poisoning by H_2S than the fuel oxidation processes that only involves CGO or the metallic phase separately. In another publication concerning only the Rh/CeO_2 catalyst system, Bunluesin *et al*. proved that smaller particle sizes (and higher dispersions) of the Rh catalyst phase gave rise to higher rates of CO oxidation (mediated by this bifunctional mechanism at low temperatures) at high CO pressures and low O_2 pressures [23]. The smaller particle size and improved dispersion of particles should increase the population density of interfacial sites between the Rh and CeO_2 phases, thus giving rise to improved kinetics for the WGSR; something that would also be expected in co-impregnated SOFC anodes, but mainly concerning the high-temperature oxidation of CO which occurs primarily on the metallic catalyst phase.

Subsequent galvanostatic operation of the SOFC in this simulated syngas mixture, containing 8 ppm H_2S (figure 7), was performed over a short period of time to mimic the breakdown of a desulfurisation unit within the HEXIS system. In this research, we allowed operation in the H_2S-containing syngas to continue for approximately four hours after the initial poisoning event, in order to determine whether the operating voltages stabilised or degraded continuously. Considering the performance of the Pt/CGO and Rh/CGO catalyst systems, this initial drop is observed and followed by a slow equilibration and stabilisation of the operating voltage, which is often observed in fuel gases with low concentrations of H_2S, due to the initial (and recoverable) chemisorption of this poisoning agent [24]. However, for the Ni/CGO

catalyst system, after the initial voltage decrease, a period of recovery is observed which begins to stabilise towards 260 minutes of operation. A tentative explanation for this slight improvement in operating voltage may relate to the formation of nickel sulfide layers at the surface of the anode 'backbone' [16], rather than bulk sulfide formation which only occurs at higher concentrations of H_2S (~3600 ppm) [8]. These layers could potentially give rise to higher catalytic activities and, in turn, performances. Gibbs free energies of metal sulfide formation (ΔG) suggest that this may be feasible for the Ni catalyst, whose sulfides form at high temperature and remain stable above 1000 °C, but not necessarily for the sulfides of the platinum group metals [25,26].

Though there are many reports on the origins of sulfur-tolerance in the literature that are relevant to this study, the exact roles of and interactions between the $LSCT_{A-}$ anode 'backbone', the impregnated CGO component and the impregnated metallic catalyst component, during operation in sulfurised gas feeds, should be determined through future *operando* spectroscopic studies of these SOFC operating in sulfur-laden fuel gases.

5. Conclusions

SOFC containing Ni/CGO, Pt/CGO and Rh/CGO co-impregnated $LSCT_{A-}$ anodes were tested in fuel streams, comprising either non-humidified H_2 or simulated syngas (2:1 H_2:CO), with up to 8 ppm H_2S, in order to determine their tolerance to poisoning by representative concentrations of sulfur-based odourising agents used in the national gas grids of Western European countries. Testing in H_2/H_2S gas mixtures showed that the Ni/CGO catalyst system was severely poisoning by H_2S, as expected, whilst the Rh/CGO system tolerated up to 2 ppm H_2S and the Pt/CGO system exhibited an improvement in ASR, even in the presence of 8 ppm H_2S. Changing the fuel to simulated syngas (2:1 H_2:CO) with 8 ppm H_2S, resulted in an increased ASR for all SOFC tested, however, during operation at 300 mA cm^{-2} for approximately four hours, the operating voltages of all SOFC stabilised and even improved over time, in the case of the Ni/CGO anode system. Overall, this research demonstrates that these metal/CGO co-impregnated $LSCT_{A-}$ anodes are capable of operating in fuel gases containing sulfur-based poisoning agents in the event of a breakdown of a desulfurisation unit, but only those that contain platinum group metal catalyst particles recover from sulfur poisoning conditions after the H_2S is removed.

Acknowledgements

The authors acknowledge funding from the University of St Andrews, HEXIS AG and the EPSRC Grants: EP/M014304/1 "Tailoring of Microstructural Evolution in Impregnated SOFC Electrodes" and EP/L017008/1 "Capital for Great Technologies".

References

[1] R. Price, M. Cassidy, J. G. Grolig, A. Mai and J. T. S. Irvine, J. Electrochem. Soc. 166 (2019) F343–F349.

[2] D. Drago, A. Lanzini and M. Santarelli, NG quality issues for use in the μ -CHP fuel cell: focus on sulfur odorants (2017).

[3] R. Price, M. Cassidy, J. A. Schuler, A. Mai and J. T. S. Irvine, ECS Trans. 68 (2015) 1499–1508.

[4] R. Price, M. Cassidy, J. A. Schuler, A. Mai and J. T. S. Irvine, ECS Trans. 78 (2017) 1385–1395.

[5] D. M. Kerrick, L. B. Eminhizer and J. F. Villaume, Am. Mineral. 58 (1973) 920–925.

[6] M. J. Jørgensen and M. Mogensen, J. Electrochem. Soc. 148 (2001) A433–A442.

[7] M. C. Verbraeken, B. Iwanschitz, A. Mai and J. T. S. Irvine, J. Electrochem Soc. 159 (2012) F757–F762.

[8] Z. Cheng, J-H. Wang, Y. Choi, L. Yang, M. C. Lin and M. Liu, Energy Environ. Sci. 4 (2011) 4380–4409

[9] Y. Matsuzaki and I. Yasuda, Solid State Ionics 132 (2000) 261–269.

[10] D. Papurello, A. Lanzini, S. Fiorilli, F. Smeacetto, R. Singh and M. Santarelli, Chem. Eng. J. 283 (2016) 1224–1233.

[11] Z. Cheng, H. Abernathy and M. Liu, J. Phys. Chem C Lett. 111 (2007) 17997–18000.

[12] A-M. Azad and M. J. Duran, Appl. Catal. A Gen. 330 (2007) 77–88.

[13] L. Y. Chen, Y. Liu, Q. Xue and M. He, J. Catal. 254 (2008) 39–48.

[14] P. Boldrin, E. Ruiz-Trejo, J. Mermelstein, J. M. Bermúdez Menéndez, T. Ramírez Reina and N. P. Brandon, Chem. Rev. 116 (2016) 13633–13684.

[15] Y. Zeng, S. Kaytakoglu and D. P. Harrison, Chem. Eng. Sci. 55 (2000) 4893–4900.

[16] H. He, R. J. Gorte, and J. M. Vohs, Electrochem. Solid State Lett. 8 (2005) A279–A280.

[17] A. Lima Da Silva and N. C. Heck, Int. J. Hydrogen Energy 40 (2015) 2334–2353.

[18] O. A. Marina, L. R. Pedersen and J. W. Stevenson, Effect of sulfur and hydrocarbon fuels on titanate/ceria SOFC anodes (2005).

[19] A. Weber, B. Sauer, A. C. Müller, D. Herbstritt and E. Ivers-Tiffée, Solid State Ionics 152–153 (2002) 543–550.

[20] A. Hagen, J. Electrochem. Soc. 160 (2013) 111–118.

[21] M. Riegraf, M. P. Hoerlein, G. Schiller and K. A. Friedrich, ACS Catal. 7 (2017) 7760–7771.

[22] T. Bunluesin, R. J. Gorte and G. W. Graham, Appl. Catal. B Environ. 15 (1998) 107–114.

[23] T. Bunluesin, H. Cortados and R. J. Gorte, J. Catal. 157 (1995) 222–226.

[24] T. R. Smith, A. Wood and V. I. Birss, Appl. Catal. A Gen. 354 (2009) 1–7.

[25] J. J. Spivey, Deactivation of reforming catalysts, in D. Shekhawat, J. J. Spivey and D. A. Berry (eds), *Fuel Cells: Technologies for Fuel Processing*. 285–315, Elsevier, Oxford (2011).

[26] D. Shekhawat, D. A. Berry, T. H. Gardner and J. J. Spivey, Reforming of liquid hydrocarbon fuels for fuel cell applications, in J. J. Spivey and K. M. Dooley (eds), *Catalysis: Volume 19*. 184–254, The Royal Society of Chemistry, Cambridge (2006).